LIMNOLOGY
and
OCEANOGRAPHY: METHODS

Limnol. Oceanogr.: Methods 4, 2006, 392–398
© 2006, by the American Society of Limnology and Oceanography, Inc.

Microorganisms in vortices: a microfluidic setup

Marcos[1] *and Roman Stocker*[2]
[1]Department of Mechanical Engineering, Massachusetts Institute of Technology, 77 Massachusetts Ave., Cambridge, MA, USA
[2]Ralph M. Parsons Laboratory, Department of Civil and Environmental Engineering, Massachusetts Institute of Technology, 77 Massachusetts Ave., Cambridge, MA, USA

Abstract

A method is presented to create microscale vortices using a microfluidic setup specifically designed to investigate the response of swimming microorganisms. Stable, small-scale vortices were generated in the side cavity of a microchannel by the shear stress in the main flow. The generation of a vortex was found to depend on the cavity's geometry, in particular its depth, aspect ratio, and opening length. Using video-microscopy, the position and orientation of individual bacteria and algae swimming in vortices of various strengths were tracked. Elongated cells were found to align with the streamlines in a strong vortex. The experimental system provides quantitative single-cell information on the interaction between microorganisms and their fluid dynamical environment.

Introduction

A wealth of results exists on motility of aquatic microorganisms in a still fluid. The wide range of swimming speeds and strategies attests to the importance of being motile in the microbial world (Fenchel 2002). Motility has acquired a new layer of ecological significance with the recognition of the role of the microbial loop and microscale patchiness on the element cycles in the ocean (Azam et al. 1983; Azam 1998). For example, swimming bacteria can exploit localized patches of enhanced nutrient concentrations (Blackburn et al. 1998), significantly increasing rates of remineralization (Fenchel 2002). On the other hand, the ocean is rarely at rest. It is therefore important to gain a quantitative understanding of the effect of the fluid dynamical environment on motility: under what conditions can swimming microbes still "determine their fate," and when do they surrender to the ambient flow?

Effects of flow on motility and chemosensory abilities of microorganisms have been investigated mainly numerically (e.g., Bowen et al. 1993, Luchsinger et al. 1999, Kiørboe and Jackson 2001). Notable exceptions are the discovery of gyrotaxis in biflagellated swimming algae (Kessler 1985) and the visualization of dinoflagellates' orientation and alignment in Couette flow (Karp-Boss et al. 2000). These studies demonstrated that novel processes are uncovered and important new insight is gained by adding flow to the microbial world. Indirect effects of the ambient flow include the role of shear stress on fertilization in the purple sea urchin (Mead and Denny 1995) and shifts in the interaction between different trophic levels under turbulence (Peters et al. 2002). On the other hand, very few experimental studies (e.g., Karp-Boss et al. 2000) have focused on the microscopic details of the effects of flow on individual microorganisms, presumably due to the difficulty in setting up accurate and controllable flow fields while visualizing and quantifying the microorganisms' response at the level of individuals.

In recent years, microfluidics has triggered important advances in a range of fields, from cellomics to chemical engineering, because of the opportunity to carefully control geometries, flows, and chemical gradients while observing the response of the system at the scale of micrometers (for reviews, see Whitesides et al. 2001, Park and Shuler 2003). Here we propose that microfluidics can represent a valuable means to study the role of flow on the motility of aquatic microorganisms quantitatively and at the level of single organisms as small as bacteria. We illustrate this by discussing a microfluidic setup to quantify the response of aquatic microorganisms to vortices of various strengths.

Eddies at the Kolmogorov scale (e.g., Yamazaki et al. 2002) are the smallest remnants of the turbulent cascade in the ocean, with time scales in the order of 1 to 100 s, depending on the intensity of turbulence (Karp-Boss et al. 1996). Kolmogorov eddies represent fluid motion at the scale most directly relevant to microbial dynamics, affecting nutrient redistribution by shear (Bowen et al. 1993, Luchsinger et al. 1999), encounter rates with predators and nutrient patches

Acknowledgments

The authors would like to thank Justin Seymour for assistance with microbiology. This work was partially funded by NSF grant OCE-0526241. Support from the Charles Reed fund is gratefully acknowledged.

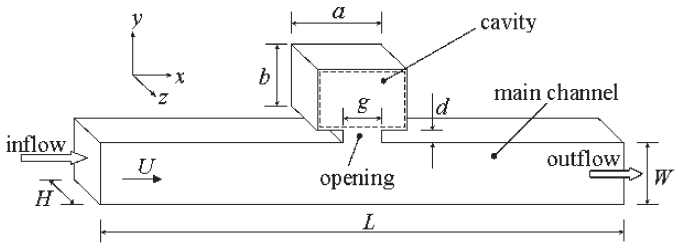

Fig. 1. Geometry of the microchannel. Gravity is in the $-z$ direction (into the plane). The cavity and the channel have the same depth, H. The dashed line shows the field of view where microorganisms are tracked. Mean velocity in the main channel is U; characteristic velocity inside the cavity is U_C.

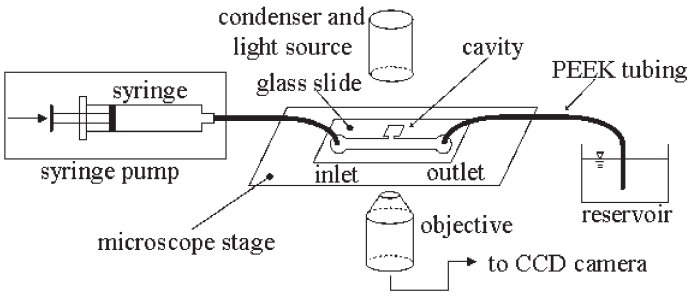

Fig. 2. Schematic of the experimental setup. The microchannel is set on the stage of an inverted microscope and flow is driven by a syringe pump. Microorganisms in the cavity are imaged with a CCD camera.

(Rothschild and Osborn 1988), and the ability of microorganisms to swim and chemotactically orient in the flow. Quantitative experimental information on microbial dynamics at these scales is still lacking. We propose to use microfluidics as a first step in understanding the response of microorganisms to microscale vortices. The generation of vortices at small Reynolds numbers has been investigated both experimentally and numerically (Higdon 1985, Shen and Floryan 1985). At the microscale, great attention has been devoted to flows that enhance mixing (e.g., Liu et al. 2000, Stroock et al. 2002), but the time scales do not reflect those relevant in the environment (e.g., Shelby et al. 2003). Yu et al. (2005) used side cavities to generate vortices in microchannels and mapped out the regime in which flow separation is to be expected. Here we apply a similar technique to generate stable microvortices on scales relevant to microbial dynamics in the aquatic environment, and show that we can obtain detailed information on the microorganisms' response.

Materials and procedures

Fabrication—Channels were fabricated using soft lithography (Whitesides et al. 2001). Fabrication begins by creating a blueprint for the microchannels using computer-aided design (CAD) software and printing it on transparency film with a high-resolution image setter to create a mask (Fineline Imaging, Colorado Springs, CO, USA). A silicon wafer is spin-coated with a layer of negative photoresist (SU8-2100; MicroChem, Newton, MA, USA), the thickness of which corresponds to the final depth of the channels. With the mask laid on the coated wafer, the latter is exposed to UV light, polymerizing exposed regions of the photoresist. After dissolving the unpolymerized photoresist, the channel structure is left on the wafer (the master). The soft polymer polydimethylsiloxane (PDMS, Sylgard 184; Dow Corning, Midland, MI, USA) is prepared according to the manufacturer's instructions and poured on the master to cast PDMS channels. After curing the PDMS by baking for 12 h at 65°C, the PDMS layer containing the channels is peeled off from the master, and holes for inlets and outlets are punched with a gauge-16 sharpened Luer tip. Finally, channels are bonded to a glass slide after treating both the PDMS layer and the glass slide with oxygen plasma for 1 min (Harrick Plasma Cleaner/Sterilizer; Harrick Scientific, Ossing, NY, USA).

Microchannel geometry—The channel has a rectangular cross section of width W and a rectangular side cavity of length a and width b (Figure 1). The depth, H, is the same for the main channel and the cavity. Differently from Yu et al. (2005), we partially closed the area between the cavity and the main channel, leaving an opening of length g. In our basic configuration, L = 10 mm, $a = W$ = 200 μm, H = 130 μm, d = 25 μm, g = 120 μm, and the cavity aspect ratio $\alpha = a/(b + d) = 1$. We also considered two additional configurations, $g = a$ = 200 μm and α = 2.

Experimental setup—The microchannel was set on the stage of a Nikon Eclipse TE2000-E inverted microscope (Nikon, Japan). PEEK tubing (0.762 mm ID, 1.59 mm OD; Upchurch Scientific, Oak Harbor, WA, USA) was used to connect the inlet to a 10-mL syringe (BD Luer-Lok Tip) via a fitting (Part P-704-01; Upchurch Scientific) and the outlet to a constant-depth reservoir, to avoid capillary and gravity effects (Figure 2). A constant flow rate in the main channel was generated using a syringe pump (PHD 2000 Programmable; Harvard Apparatus, Holliston, MA, USA). For the appropriate geometrical configuration, the shear stress of the main flow produced a vortex in the cavity of strength proportional to the mean velocity U in the main channel.

The flow field within the channel was visualized using 2-μm diameter beads (Polysciences, Warrington, PA, USA). Phase contrast was used to image the beads and the microorganisms, with long-working-distance ×20 (Numerical Aperture [NA] = 0.45) and ×40 (NA = 0.6) objectives. The depth of field can be calculated following Meinhart et al. (2000): for 2-μm beads, we obtained 28 μm (×20) and 19 μm (×40). Sequences of images (movies) were captured with a 1600-by-1200-pixel, 14 bit, cooled CCD camera (pixel size 7.4 by 7.4 μm^2, PCO 1600; Cooke, Romulus, MI, USA) at 30 to 62 frames per second and processed using IPLab software (Scanalytics, Fairfax, VA, USA). In the images, beads or microorganisms appear as bright regions on a darker background. Images of the trajectories were obtained by assigning to each pixel the maximum light intensity recorded in that pixel over the duration of the movie ("3D Time Stacked View" command in IPLab).

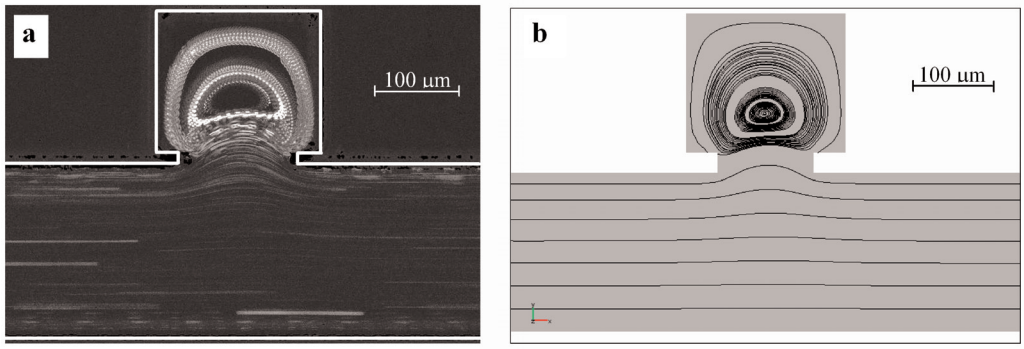

Fig. 3. The flow in a cavity of aspect ratio $\alpha = 1$, main flow speed $U = 21.4$ mm s^{-1}. The characteristic velocity in the cavity is $U_C = 363$ μm s^{-1}. Lengths of the cavity and the opening are $a = 200$ μm and $g = 120$ μm, respectively. Flow is from left to right. The cavity Reynolds number ($U_C a/\nu$) is 0.07. (a) Trajectories of 2-μm beads. The solid white line shows the outline of the channel. (b) Numerical streamlines at the mid-depth plane ($z = H/2 = 65$ μm). Imperfections in the streamlines result from small numerical errors in integrating the velocity field.

Numerical modeling—For preliminary screening of a range of design configurations, as well as for accurate characterization of the flow field, we carried out a computational fluid dynamics simulation of the cavity flow. We used the finite-element code Comsol Multiphysics (Burlington, MA, USA) to solve the steady-state Navier-Stokes equations in 3-dimensional space. The model geometry was that described above, except for $L = 1$ mm to save computational time (we verified that the flow field in the cavity is the same as for $L = 10$ mm). The boundary conditions were no-slip on all solid boundaries, uniform velocity at the inflow, and zero pressure at the outflow. We adopted a multigrid solver using between 13,000 and 22,000 elements, each at most 30 μm in size.

Microorganisms—The marine bacterium *Pseudoalteromonas haloplanktis* (2 μm length) was grown to exponential phase in 1% tryptic soy broth (TSB) at room temperature, before being diluted 1:10 in artificial seawater. Experiments were performed 72 h later. The motile marine alga *Dunaliella tertiolecta* (5 μm diameter) was grown to exponential phase in f/2 medium.

Assessment and discussion

Generation of a vortex—Using the setup described above we were able to generate a stable and reproducible vortex in a cavity of aspect ratio $\alpha = 1$ (Figure 3a). The numerical streamlines (Figure 3b) closely match the experimental trajectories, as expected for a steady flow. Good agreement is further demonstrated by comparing the velocity measured experimentally with its numerical counterpart at different locations in the cavity (Figure 4). We can therefore use the numerical model to investigate the vortex in more detail. For our geometry, the maximum velocity in the cavity is $U_C = 1.7\%\ U$ for a main-channel Reynolds number $\mathrm{Re} = UW/\nu < 6$ (where ν is the kinematic viscosity), corresponding to $U < 30$ mm s^{-1}. In contrast to higher Reynolds number designs (e.g., Shelby et al. 2003), generation of the vortex does not rely on inertial effects. Whereas the flow inside the cavity is in principle 3 dimensional, the vertical velocity (along z) is always much smaller than the horizontal velocity at the mid-depth plane, where all observations are made.

Effects of the cavity geometry—Because of the fabrication processes involved in soft lithography, shallower channels are easier and faster to fabricate and, in general, the depth H is limited to about 1 mm. On the other hand, a minimum depth is required to generate a vortex. For our basic configuration, a vortex starts to form for $H = 80$ μm (not shown) and is fully developed for $H \geq 90$ μm ($= 0.45\ a$; Figure 5b).

It is interesting to note that this minimum depth changes with the cavity opening length g, not considered in previous studies. It has been shown that a 2-dimensional flow (i.e., $H \to \infty$) in a fully open cavity ($g = a$) generates a vortex for aspect ratios $\alpha < 2$ (Higdon 1985, Shen and Floryan 1985, Yu et al. 2005). In 3-dimensional low Reynolds number flow ($\mathrm{Re}^* = \mathrm{Re}\ A_C < 10$), however, a vortex is expected only for $A_C = (H/a)^2 > 0.327$, predicting a minimum depth $H = 0.57a$ for $\mathrm{Re} < 30.6$ (Yu et al. 2005). We confirmed this prediction numerically by testing

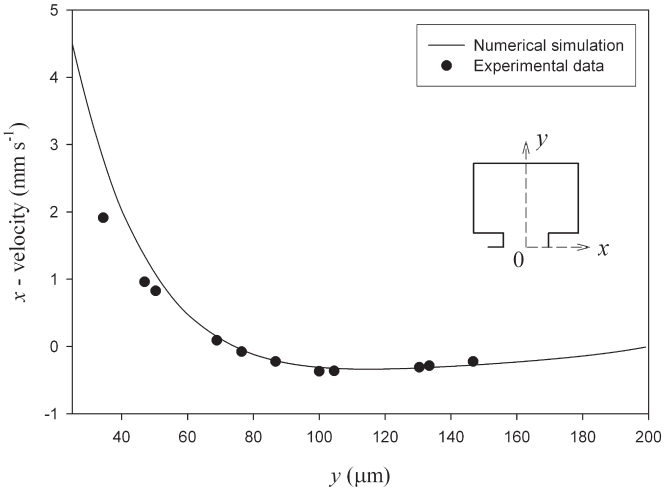

Fig. 4. Velocity inside the cavity in the x– direction, as a function of the transverse position y (dashed line in the inset) for $U_C = 363$ μm s^{-1}. Experiments (circles) are compared with numerical results (solid line).

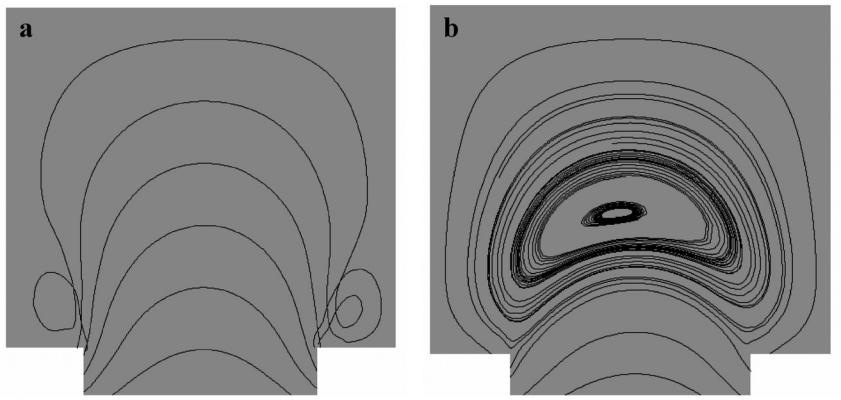

Fig. 5. Numerical streamlines for $U = 21.4$ μm s^{-1} and 2 different depths: (a) $H = 70$ μm; (b) $H = 90$ μm. All other dimensions are as in Figure 3. Crossing streamlines visible in panel a reflect small 3-dimensional effects.

the case $g = a$ for $H = 90$ μm ($A_C = 0.203$, Re* = 1.25), finding indeed no vortex. Partially closing the cavity opening g, on the other hand, introduces an additional degree of freedom, which we discovered reduces the minimum depth required for vortex formation. This can be seen by comparing Figure 3 ($g = 120$ μm; a vortex forms) with Figure 6a ($g = 200$ μm; no vortex), both obtained with $H = 130$ μm. Finally, no vortex formed for $\alpha = 2$, even for $g = a/2$ (Figure 6b).

Trajectories and orientation of swimming microorganisms—Our aim in designing the cavity flow was to obtain a controlled, well-characterized flow field to study the response of microorganisms. In the previous sections, we have analyzed the formation of the vortex numerically and experimentally. Here we show that this setup also allows accurate visualization and quantification of the trajectories and instantaneous orientation of microorganisms swimming in the vortex, by applying it to the marine bacterium *P. haloplanktis* and the marine alga *D. tertiolecta*.

To have only motile organisms inside the cavity, we prefilled the channel with fluid, injected the microorganisms, then stopped the flow: this procedure allowed some motile cells to spontaneously enter the cavity, at which point the flow was turned on again. Trajectories were imaged in the field of view shown in Figure 1 (dashed line) at mid-depth ($z = H/2$). A ×40 objective was used for the bacteria and a ×20 objective for the algae. No effect of the microscope light on the microorganisms was observed.

In the absence of flow (Figure 7a), *P. haloplanktis* swims in a random fashion, exhibiting a combination of long, straight runs, reversals, and changes of direction, with a mean speed of 55 μm s^{-1} and a maximum of 280 μm s^{-1}. When the flow velocity in the vortex is considerably larger than the swimming speed (Figure 7c), advection by the flow overwhelms motility and trajectories tend to streamlines. The elongated shape of *P. haloplanktis*, characteristic of many species of bacteria, also allows detection of its orientation in the flow field. In a strong vortex, bacteria not only follow streamlines, but they are aligned with them as a result of the shear in the vortex (Figure 7e), except for the corner regions in the cavity, which the vortex

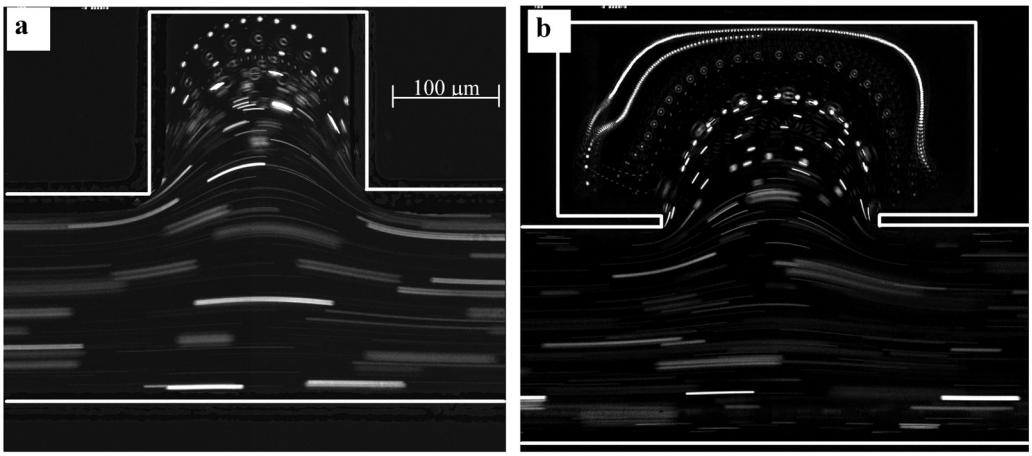

Fig. 6. Two configurations in which no vortex formed, as shown by the trajectories of 2-μm beads: (a) $\alpha = 1$, $g = a = 200$ μm; (b) $\alpha = 2$, $g = a/2 = 200$ μm. For both cases, $H = 130$ μm and $U = 21.4$ mm s^{-1}. The scale is the same in the 2 panels.

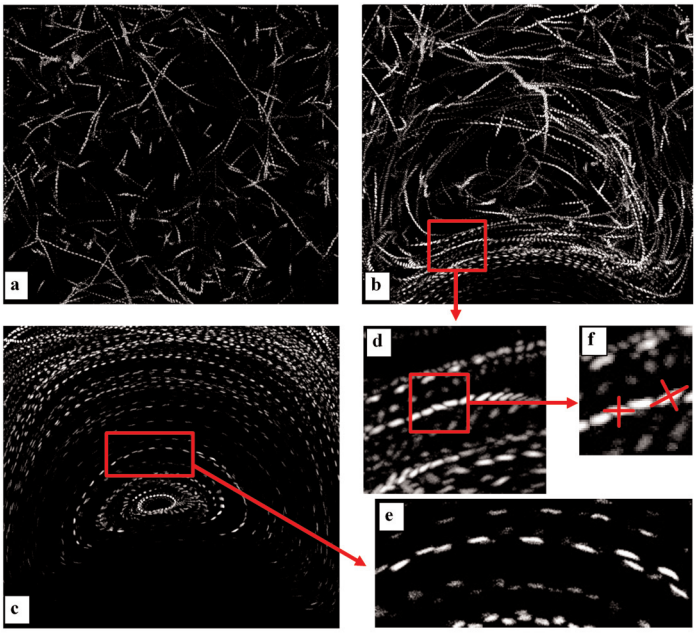

Fig. 7. Trajectories of the bacteria *P. haloplanktis* in vortices of different strength: (a) No flow; (b) $U_C = 36.3$ μm s^{-1}; (c) $U_C = 363$ μm s^{-1}. The field of view is shown in Figure 1; d and e are magnified views of selected trajectories, showing the instantaneous orientations of individual bacteria; in f, a bacterium's orientation is further magnified to highlight misalignment with the direction of travel.

does not reach (e.g., the top corners in Figure 7c). The most interesting case is that of a vortex of intermediate strength (Figure 7b), where bacteria can partially "fight the flow": several trajectories cross streamlines and, even for those that do not, the shear is not strong enough to always align bacteria with the flow direction (Figures 7d and 7f).

We further applied the microfluidic setup to the motile alga *D. tertiolecta* (Figure 8), which swims up to 375 μm s^{-1} using two flagella. Its large size (5 μm) makes it easy to capture using video-microscopy, but its instantaneous orientation is more difficult to quantify due to its nearly symmetrical shape. Many species of phytoplankton in the ocean are known to use motility for phototaxis or chemotaxis, resulting in migration and clustering in preferential regions of the water column (Sjoblad et al. 1978, Eggersdorfer and Hader 1991). Phytoplankton motility is altered by small-scale vortices, and the proposed setup can help to quantify these changes (Figure 8b).

A preliminary quantification of the role of advection on motility can be obtained by visual inspection of the trajectories and is summarized in Table 1. Motility of *P. haloplanktis* is not significantly affected for $U_C < 36$ μm s^{-1}, whereas advection dominates for $U_C > 182$ μm s^{-1}. *D. tertiolecta*, on the other hand, can swim faster and exhibits higher thresholds (182 to 363 μm s^{-1}) before being passively advected by the flow. In the ocean, turbulent dissipation rates ε range from 10^{-2} to 10^{-5} cm^2 s^{-3} (Lazier and Mann 1989), corresponding to Kolmogorov velocity scales of 1000 to 178 μm s^{-1} (Yamazaki et al. 2002), respectively. While the main purpose of this calculation is to demonstrate the viability of the experimental setup and not to provide a thorough quantitative analysis of the data, Table 1 suggests that bacteria would be mostly advected and aligned in a turbulent flow, whereas motile algae can overcome mild turbulence levels.

Shear flows affect the orientation of elongated bodies. Rigid spheroids undergo periodic rotation depending on their axis ratio (Jeffery 1922). In the case of swimming bacteria, orientation is governed by motility in addition to shear, and no theoretical prediction is available. We quantified the effects of shear on the ability of *P. haloplanktis* to control its orientation by determining the angle of misalignment between a bacterium and its instantaneous trajectory. The orientation θ_B of the bacterium is defined as the angle formed by its major axis with the x-axis (Figure 9d). The instantaneous orientation θ_T of its trajectory (governed by a combination of swimming and advection)

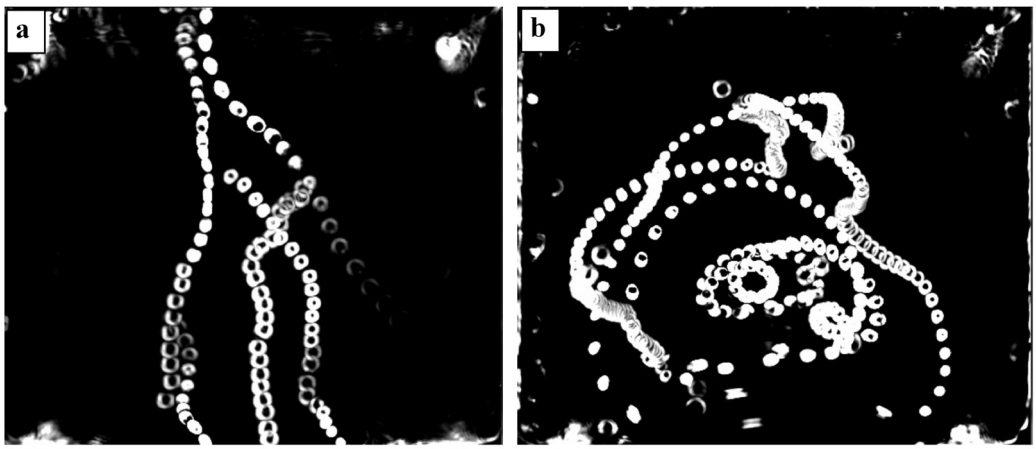

Fig. 8. Trajectories of the alga *D. tertiolecta* swimming in the cavity: (a) No flow; (b) $U_C = 363$ μm s^{-1}. The field of view is shown in Figure 1. The black spot inside each alga is a result of phase contrast microscopy.

Table 1. The influence of advection on *P. haloplanktis* and *D. tertiolecta* in vortices of various strengths.

U_c μm s^{-1}	ε, cm^2 s^{-3}	*P. haloplanktis* (bacterium)	*D. tertiolecta* (alga)
9	6.8×10^{-11}	– –	– –
18	1.1×10^{-9}	– –	– –
36	1.7×10^{-8}	–	– –
91	6.8×10^{-7}	+	–
182	1.1×10^{-5}	++	+
363	1.7×10^{-4}	++	+

An equivalent dissipation rate ε is calculated based on U_c. Symbols indicate the importance of advection by the vortex over motility as inferred from trajectories, from ++ (advection dominates) to – – (motility dominates).

is computed from the bacterium's position time series using center differences. The misalignment angle is then $\Delta\theta = |\theta_B - \theta_T|$ (Figure 9d), with the constraint $0° \le \Delta\theta \le 90°$ since we cannot distinguish between fore and aft in the bacterium's orientation. Locations and orientations of the bacteria were obtained using Java software (BacTrack) developed in-house. After successfully testing the algorithm against artificial data, we applied it to the 3 experiments shown in Figures 7a-c: the resulting probability distributions (pdf) for Δθ are shown in Figures 9a-c, respectively. In the absence of flow, *P. haloplanktis* shows a broad distribution of misalignment angles, with some preference to be aligned in the direction of swimming (Figure 9a). The vortex of intermediate strength (Figure 9b) misaligns some bacteria with respect to their trajectories, but is not strong enough to trigger a consistent alignment with streamlines, resulting in a flattening of the Δθ distribution. For the strongest vortex, the large peak at small values of Δθ shows that alignment with streamlines is predominant (Figure 9c). While these effects and their ecological significance will be further explored in a separate contribution, these data confirm the viability of the proposed method to obtain single-cell quantitative information on the effect of the fluid dynamical environment on microorganisms as small as bacteria.

Comments and recommendations

We presented a microfluidic setup to generate vortices on scales relevant to microbial dynamics, while at the same time tracking responses of individual swimming microorganisms. We found that the formation of a vortex in the side cavity depends on the depth-to-width ratio (*H/a*) of the cavity, as well as the length of the opening (*g*) to the main channel.

We illustrated the ability of the setup to yield quantitative single-cell information on the behavior of microbes exposed to a recirculating shear flow. Steady flow in the cavity is only an approximation of Kolmogorov-scale eddies in the ocean, which are 3-dimensional and unsteady (Karp-Boss et al. 1996), with time scales in the order of 1 to 100 s. Although it would be possible to incorporate unsteadiness by modulating the flow in the microchannel over time using a programmable

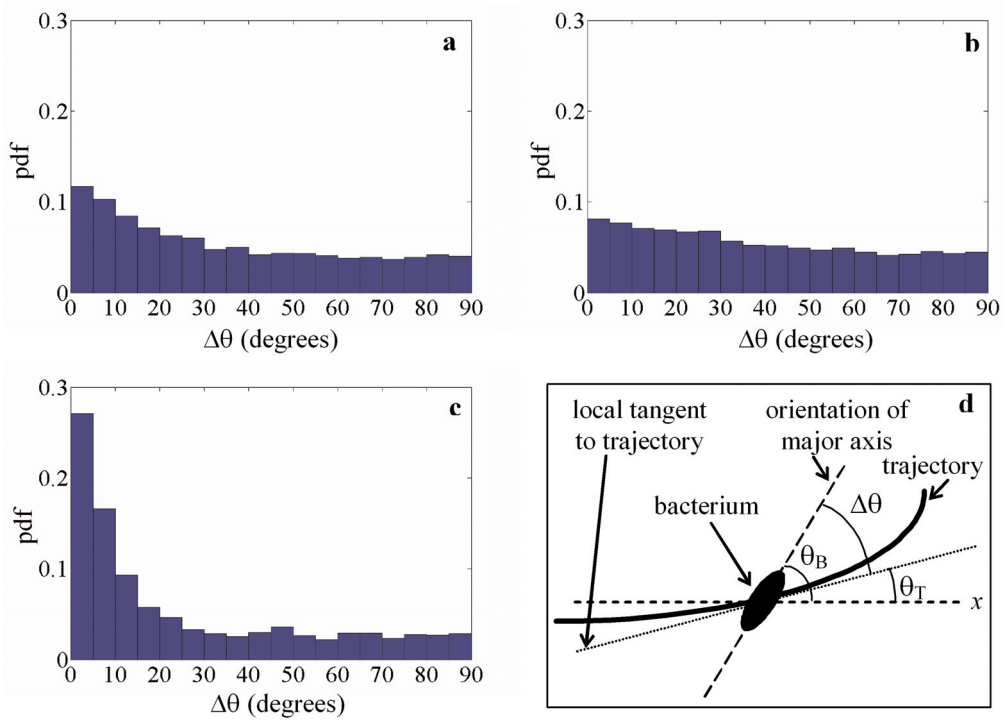

Fig. 9. Probability distribution (pdf) of the misalignment angle Δθ (defined in panel d) of *P. haloplanktis* for the 3 cases shown in Figure 7: (a) No flow; (b) U_c = 36.3 μm s^{-1}; (c) U_c = 363 μm s^{-1}.

syringe pump, we believe the current setup in itself offers valuable insight on the fundamental interaction between microorganisms and their fluid dynamical environment (in particular the mean shear) at scales relevant to microbial dynamics, at least over times shorter than the Kolmogorov time-scale.

We envisage that microfluidic methods such as the one presented here will provide novel insight into the bounds that ambient flow imposes on the motility of microorganisms and on the behavioral strategies and dynamics of motile microbes living in a turbulent ocean. They will in turn impact our understanding of the role of microorganisms in the biogeochemistry of aquatic environments.

References

Azam, F., T. Fenchel, J. G. Field, J. S. Gray, L. A. Meyer-Reil, and F. Thingstad. 1983. The ecological role of water-column microbes in the sea. Mar. Ecol. Prog. Ser. 10:257-263.

———. 1998. Microbial control of oceanic carbon flux: The plot thickens. Science 280:694-696.

Blackburn, N., T. Fenchel, and J. Mitchell. 1998. Microscale nutrient patches in planktonic habitats shown by chemotactic bacteria. Science 282:2254-2256.

Bowen, J. D., K. D. Stolzenbach, and S. W. Chisholm. 1993. Simulating bacterial clustering around phytoplankton cells in a turbulent ocean. Limnol. Oceanogr. 38:36-51.

Eggersdorfer, B. and D. P. Hader. 1991. Phototaxis, gravitaxis and vertical migrations in the marine dinoflagellate prorocentrum-micans. FEMS Microbiol. Ecol. 85:319-326.

Fenchel T. 2002. Microbial behaviour in a heterogenous world. Science 296:1068-1071.

Higdon, J. J. L. 1985. Stokes flow in arbitrary two-dimensional domains: shear flow over ridges and cavities. J. Fluid Mech. 159:195-226.

Jeffery, G. B. 1922. The motion of ellipsoidal particles immersed in a viscous fluid. Proc. R. Soc. Lond. 102:161-179.

Karp-Boss, L., E. Boss, and P. A. Jumars. 1996. Nutrient fluxes to planktonic osmotrophs in the presence of fluid motion. Oceanogr. Mar. Biol. Ann. Rev. 34:71-107.

———, E. Boss, and P. A. Jumars. 2000. Motion of dinoflagellates in a simple shear flow. Limnol. Oceanogr. 45: 1597-1602.

Kessler, J. O. 1985. Hydrodynamic focusing of motile algal cells. Nature 313:218.

Kiørboe, T., and G. A. Jackson. 2001. Marine snow, organic solute plumes, and optimal chemosensory behavior of bacteria. Limnol. Oceanogr. 46:1309-1318.

Lazier, J. R. N., and K. H. Mann. 1989. Turbulence and the diffusive layers around small organism. Deep-Sea Res. 36: 1721-1733.

Liu, R. H., M. A. Stremler, K. V. Sharp, M. G. Olsen, J. G. Santiago, R. J. Adrian, H. Aref, and D. J. Beebe. 2000. Passive mixing in a three-dimensional serpentine microchannel. J. Microelectromech. Syst. 9:190-197.

Luchsinger, R. H., B. Bergersen, and J. G. Mitchell. 1999. Bacterial swimming strategies and turbulence. Biophys. J. 77: 2377-2386.

Mead, K. S., and M. W. Denny. 1995. The effects of hydrodynamic shear stress on fertilization and early development of the purple sea urchin *Strongylocentrotus purpuratus*. Biol. Bull. 188:46-56.

Meinhart, C. D., S. T. Wereley, and M. H. B. Gray. 2000. Volume illumination for two-dimensional particle image velocimetry. Meas. Sci. Technol. 11:809-814.

Park, T. H., and M. L. Shuler. 2003. Integration of cell culture and microfabrication technology. Biotechnol. Prog. 19:243-253.

Peters, F., C. Marrase, H. Havskum, F. Rassoulzadegan, J. Dolan, M. Alcaraz, and J. M. Gasol. 2002. Turbulence and the microbial food web: effects on bacterial losses to predation and on community structure. J. Plankton Res. 24:321-331.

Rothschild, B. J., and T. R. Osborn. 1988. Small-scale turbulence and plankton contact rates. J. Plankton Res. 10:465-474.

Shelby, J. P., D. S. W. Lim, J. S. Kuo, and D. T. Chiu. 2003. High radial acceleration in microvortices. Nature 425:38.

Sjoblad, R. D., I. Chet, and R. Mitchell. 1978. Quantitative assay for algal chemotaxis. Appl. Environ. Microbiol. 36:847-850.

Shen, C., and J. M. Floryan. 1985. Low Reynolds number flow over cavities. Phys. Fluids 28:3191-3202.

Stroock, A. D., S. K. W. Dertinger, A. Ajdari, I. Mezic, H. A. Stone, and G. M. Whitesides. 2002. Chaotic mixer for microchannels. Science 295:647-651.

Whitesides, G. M., E. Ostuni, S. Takayama, X. Jiang, and D. E. Ingber. 2001. Soft Lithography in biology and biochemistry. Annu. Rev. Biomed. Eng. 3:335-373.

Yamazaki, H., D. L. Mackas, and K. L. Denman. 2002. Coupling small-scale physical processes with biology. Sea 12: 51-112.

Yu, Z. T. F., Y.-K. Lee, M. Wong, and Y. Zohar. 2005. Fluid flows in microchannels with cavities. J. Microelectromech. Syst. 14:1386-1398.

Submitted 19 April 2006
Revised 11 September 2006
Accepted 22 September 2006